Origin of interfacial polar order in incipient ferroelectrics

Yijia Gu, Nan Wang, Fei Xue, and Long-Qing Chen
Department of Materials Science and Engineering, The Pennsylvania State University, University Park, Pennsylvania 16802, USA
(Received 13 February 2015; published 11 May 2015)

There are ample experimental evidences indicating that the ferroelastic domain walls of incipient ferroelectrics, such as $SrTiO_3$ and $CaTiO_3$, are polar. The emergence of such interfacial polar order at a domain wall is exciting and believed to arise from the coupling between a primary order parameter, such as a strain or an antiferrodistortive (AFD) order parameter, and polarization. There have been several mechanisms proposed to explain the emergence of interfacial polar order, including biquadratic coupling, AFD-antiferroelectric coupling, and flexoelectric coupling. Using $CaTiO_3$ as an example, we demonstrate, using both asymptotic analytics and numerical calculation, that the flexoelectric coupling is likely the dominant mechanism leading to the interfacial polar order.

DOI: 10.1103/PhysRevB.91.174103 PACS number(s): 77.84.−s, 77.80.Dj, 68.35.−p

All ferroic transitions lead to the formation of domains separated by domain walls. The overall responses of a ferroic solid are often strongly influenced by the behavior of domain walls. As a matter of fact, domain walls may possess more intriguing properties than the bulk domains, for instance, high electronic conductivity [1–4], chirality [5,6], and oxygen vacancy segregation [7,8] in ferroelectric domain walls and polar domain walls arising from incipient ferroelectrics [9–14]. It was even suggested [15] that the domain walls of ferroelectrics may be treated as new engineering elements of multifunctional materials.

Domain walls have been extensively studied both experimentally [2,10,16–23] and theoretically [4,5,12,24–34]. In particular, the classic continuum Landau-Ginzburg-Devonshire (LGD) theory has been extensively employed to analyze both ferroelectric properties of single domains and domain walls [35,36]. It has recently been extended to study the phenomena involving multiple order parameters at nanometer scale such as domain walls, and the results show good agreement with atomistic scale calculations [6,37–39]. Many ferroic oxides exhibit multiple instabilities described by different soft modes or order parameters, and it is the coupling among the order parameters that yields numerous interesting phenomena such as polar domain walls in incipient ferroelectrics, incommensurate domain patterns, and improper ferroelectrics. To account for the interactions among order parameters, several forms of couplings have been proposed in LGD theory including biquadratic, trilinear, and flexoelectric terms. For instance, the biquadratic coupling is a general symmetry-allowed term that describes competition between two order parameters [5]; the trilinear coupling leads to improper ferroelectrics [40]; and the flexoelectric coupling produces incommensurate domain patterns [41]. However, the relative contributions of these couplings to the structures and properties of domain walls remain unclear. In this paper, we study the domain walls of $CaTiO_3$ as an example to discuss the roles of each aforementioned coupling term to the domain walls. In particular, we demonstrate that the polar domain wall in $CaTiO_3$ is most likely to be induced by flexoelectric coupling.

At ambient temperature and pressure, $CaTiO_3$ has an orthorhombic distorted-perovskite structure with space group *Pbnm*. Disregarding the minor distortion of TiO_6 octahedra, the structure of $CaTiO_3$ can be illustrated as a combination of two kinds of TiO_6 octahedral tilts: two out-of-phase tilts around the x_1 and x_2 axes, and one in-phase tilt around the x_3 axis (Glazer's notation $a^-a^-c^+$). (In this paper, the coordinate system is chosen along the crystallographic directions of the pseudocubic lattice.) These two kinds of tilts can also be used as order parameters to characterize the antiferrodistortive (AFD) transitions in $CaTiO_3$ [42]. $CaTiO_3$ may form several kinds of twin walls, or ferroelastic domain walls, among which the (110) twinned structures, as schematically plotted in Fig. 1, are the most common and intensively studied. It is shown both experimentally and theoretically that the twin wall is polar. With aberration-corrected transmission electron microscopy, the displacement pattern of Ca and Ti at the domain wall is observed, which indicates nonzero polarization along the x_2 direction [11]. A recent confocal second harmonic generation experiment also confirms the polar nature of the $CaTiO_3$ twin walls [13]. Theoretical calculations showed similar predictions as well. From molecular dynamics [14] and first-principles calculations [12], it is found the polarization direction is associated with the twin wall angle, as indicated by the red arrows in Fig. 1. In addition to the x_2 direction polarization, it is shown that there exists additional antiferroelectric (AFE)-like polarization distribution along the x_1 direction by the molecular dynamics [14], first-principles calculations [12], and the LGD theory [4]. Such a complicated polarization configuration inside the twin wall has been attributed to the improper AFD-AFE coupling [12], flexoelectric coupling [4], or the biquadratic coupling [5] by different research groups.

In this paper, we first employ the LGD theory in combination with the phase-field method to elucidate the underlying thermodynamic driving forces leading to the formation of polar domain walls in $CaTiO_3$. We solve the state equations of LGD theory and thus get the equilibrium values of order parameters using the phase-field method [43]. The domain structure in the phase-field model is described by the spatial distribution of order parameters (Q_i) that include spontaneous electric polarization (P_i), out-of-phase tilt (φ_i), and in-phase tilt (θ_i) in the case of $CaTiO_3$. The temporal evolution of the order parameters is described by time-dependent Ginzburg-Landau equations

$$\frac{\partial Q_i}{\partial t} = -L\frac{\delta F}{\delta Q_i} \quad (i = 1,2,3), \tag{1}$$

where L is the kinetic coefficient related to the mobility of domain walls. F is the volume integral of free energy density, which includes bulk free energy, gradient energy, elastic energy, and electrostatic energy. With biquadratic coupling, the free energy density is

$$\begin{aligned} f(P_i,\varphi_i,\theta_i,\varepsilon_{ij},E_i) = {} & \alpha_{ij}P_iP_j + \alpha_{ijkl}P_iP_jP_kP_l + \alpha_{ijklmn}P_iP_jP_kP_lP_mP_n - \mu_{ijkl}\varphi_i\varphi_j\theta_k\theta_l + \beta_{ij}\varphi_i\varphi_j + \beta_{ijkl}\varphi_i\varphi_j\varphi_k\varphi_l \\ & + \beta_{ijklmn}\varphi_i\varphi_j\varphi_k\varphi_l\varphi_m\varphi_n - \kappa_{ijkl}P_iP_j\theta_k\theta_l + \gamma_{ij}\theta_i\theta_j + \gamma_{ijkl}\theta_i\theta_j\theta_k\theta_l + \gamma_{ijklmn}\theta_i\theta_j\theta_k\theta_l\theta_m\theta_n \\ & - t_{ijkl}P_iP_j\varphi_k\varphi_l + \frac{1}{2}\xi_{ijkl}\left(\frac{\partial P_i}{\partial x_j}\frac{\partial P_k}{\partial x_l}\right) + \frac{1}{2}\upsilon_{ijkl}\left(\frac{\partial \varphi_i}{\partial x_j}\frac{\partial \varphi_k}{\partial x_l}\right) + \frac{1}{2}\omega_{ijkl}\left(\frac{\partial \theta_i}{\partial x_j}\frac{\partial \theta_k}{\partial x_l}\right) \\ & + \frac{1}{2}s_{ijkl}\sigma_{ij}\sigma_{kl} - Q_{ijkl}\sigma_{ij}P_kP_l - R_{ijkl}\sigma_{ij}\varphi_k\varphi_l - G_{ijkl}\sigma_{ij}\theta_k\theta_l - P_iE_j - \frac{1}{2}\varepsilon_0\kappa^b_{ij}E_iE_j, \end{aligned} \tag{2}$$

where α, β, and γ are Landau-Devonshire coefficients (only the coefficients of the second order terms are temperature dependent); ξ_{ijkl}, υ_{ijkl}, and ω_{ijkl} are the anisotropic gradient energy coefficients of polarization, out-of-phase tilt, and in-phase tilt, respectively; t_{ijkl}, κ_{ijkl}, G_{ijkl}, μ_{ijkl}, Q_{ijkl}, and R_{ijkl} are coupling coefficients; s_{ijkl} is the elastic compliance tensor; σ_{ij} is the stress; E_i is the external electric field; ε_0 is the dielectric permittivity of vacuum; and κ^b_{ij} is the background dielectric constant. All of the coefficients can be found in Ref. [42].

Phase-field simulations using the free energy expression (2) are performed to examine the effect of biquadratic coupling between the structural order parameters (φ and θ) and its possible role in the generation of polar domain walls. The simulation system setup also follows Fig. 1. It includes three domains and two domain walls. The domain walls lie in the x_2-x_3 plane and are perpendicular to the x_1 direction. To compare with the existing results of $CaTiO_3$ domain walls, we choose the same twin structure as in previous papers [11,12,14]. The order parameters in domains I, II, and III are therefore $(\varphi_1, \varphi_2, \theta_3)$, $(-\varphi_1, \varphi_2, \theta_3)$, and $(\varphi_1, \varphi_2, \theta_3)$, respectively. The system is then simplified to a one-dimensional problem with the simulation size $4096\Delta x \times 1\Delta x \times 1\Delta x$ using the three-dimensional phase-field model. The grid size Δx is chosen to be 0.25 nm. Periodic boundary condition is imposed along each direction. The stress field is calculated using Khachaturyan's microelastic theory [44], and the electric depolarization field is obtained by solving Poisson's equation [45]. To get the designed twin structures, we start our simulation with the preassigned order parameter values ($P_1 = P_2 = 0.1\,\mathrm{C/m^2}$, and $\varphi_1 = \varphi_2 = -\theta_3 = -5$ pm), and then let the system relax to equilibrium. The calculated equilibrium values for the structural order parameters are 5.64 and 5.89 pm for the out-of-phase tilt component and in-phase tilt component, respectively. These values agree well with the literature [12,46,47]. The calculated angle between the two domains is 178.8°, which is identical to experimental observations [11]. However, no polarization is observed at the domain wall and throughout the whole simulation system.

Since the phase-field numerics above may be sensitive to the coefficients of the free energy, a generalized near-interface asymptotic analysis [48] of the phase-field model with biquadratic coupling is also carried out here to support our conclusion. First, to simplify analytics, the electrostatic contribution is ignored. The total free energy with up to fourth order terms is then

$$\begin{aligned} f^B(P_1,P_2,\varphi_1,\varphi_2,\theta_3) = {} & \alpha_1\left(P_1^2+P_2^2\right) + \alpha_{11}\left(P_1^2+P_2^2\right)^2 + \alpha_{12}\left(P_1^4+P_2^4\right) - \mu_{12}\left(\varphi_1^2+\varphi_2^2\right)\theta_3^2 + \beta_1\left(\varphi_1^2+\varphi_2^2\right) \\ & + \beta_{11}\left(\varphi_1^2+\varphi_2^2\right)^2 + \beta_{12}\left(\varphi_1^4+\varphi_2^4\right) - \kappa_{12}\left(P_1^2+P_2^2\right)\theta_3^2 + \gamma_1\theta_3^2 + (\gamma_{11}+\gamma_{12})\theta_3^4 \\ & - t_{11}\left(P_1^2\varphi_1^2+P_2^2\varphi_2^2\right) - t_{12}\left(P_1^2\varphi_2^2+P_2^2\varphi_1^2\right) - t_{44}P_1P_2\varphi_1\varphi_2 - (G_{12}\sigma_{22}+G_{11}\sigma_{33})\theta_3^2 \\ & - \left[Q_{12}\sigma_{22}P_1^2 + Q_{11}\sigma_{22}P_2^2 + Q_{12}\sigma_{33}\left(P_1^2+P_2^2\right)\right] - \left[R_{12}\sigma_{22}\varphi_1^2 + R_{11}\sigma_{22}\varphi_2^2 + R_{12}\sigma_{33}\left(\varphi_1^2+\varphi_2^2\right)\right] \\ & + \tfrac{1}{2}\xi_{11}P_{1,1}^2 + \tfrac{1}{2}\xi_{44}P_{2,1}^2 + \tfrac{1}{2}\upsilon_{11}\varphi_{1,1}^2 + \tfrac{1}{2}\upsilon_{44}\varphi_{2,1}^2 + \tfrac{1}{2}\omega_{44}\theta_{3,1}^2 + \tfrac{1}{2}s_{11}\left(\sigma_{22}^2+\sigma_{33}^2\right) + s_{12}\sigma_{22}\sigma_{33}, \end{aligned} \tag{3}$$

where the two nonzero stress components are given by

$$\sigma_{22} = \frac{U_2s_{11} - U_3s_{12}}{s_{11}^2 - s_{12}^2}, \quad \sigma_{33} = \frac{U_3s_{11} - U_2s_{12}}{s_{11}^2 - s_{12}^2}, \tag{4}$$

with $U_2 = R_{12}[(\varphi_1^e)^2 - \varphi_1^2] - Q_{12}P_1^2 - Q_{11}P_2^2$ and $U_3 = R_{12}[(\varphi_1^e)^2 - \varphi_1^2] - Q_{12}(P_1^2 + P_2^2)$. It should be mentioned that these two stress components are zero inside the domain, while nonzero near the wall. Bulk equilibrium values of the order parameters in the domains are φ_1^e, φ_2^e, and θ_3^e. Minimizing the total free energy with respect to polarization P_1 and P_2, one can easily get

$$2P_1\left[Q_{12}(\sigma_{22}+\sigma_{33}) + \alpha_1 + \alpha_{11}\left(P_1^2+P_2^2\right) + 2\alpha_{12}P_1^2 - t_{11}\varphi_1^2 - t_{12}\varphi_2^2 - \kappa_{12}\theta_3^2\right] - \xi_{11}\frac{\partial^2 P_1}{\partial x_1^2} = t_{44}P_2\varphi_1\varphi_2 \tag{5a}$$

$$2P_2\left[Q_{11}\sigma_{22} + Q_{12}\sigma_{33} + \alpha_1 + \alpha_{11}\left(P_1^2+P_2^2\right) + 2\alpha_{12}P_2^2 - t_{11}\varphi_2^2 - t_{12}\varphi_1^2 - \kappa_{12}\theta_3^2\right] - \xi_{44}\frac{\partial^2 P_2}{\partial x_1^2} = t_{44}P_1\varphi_1\varphi_2. \tag{5b}$$

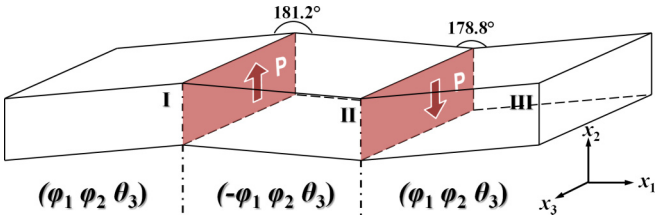

FIG. 1. (Color online) The schematic of the simulation system. There are three domains, I, II, and III with two twin walls. The corresponding order parameters are shown for each domain. The coordinate system is chosen along crystallographic directions of the pseudocubic lattice.

Near the domain wall, one can write order parameters in terms of their deviation from bulk value $\varphi_1 = \varphi_1^e + \delta\varphi_1$, $P_1 = \delta P_1$, and $P_2 = \delta P_2$. Assuming all the deviations are at the same order, expanding Eq. (5) to the first order of small deviation leads to

$$\begin{aligned} &2\delta P_1\left[\alpha_1 - t_{11}\left(\varphi_1^e\right)^2 - t_{12}\left(\varphi_2^e\right)^2 - \kappa_{12}\left(\theta_3^e\right)^2\right] - \xi_{11}\frac{\partial^2\delta P_1}{\partial x_1^2} \\ &\quad = t_{44}\delta P_2\varphi_1^e\varphi_2^e \\ &2\delta P_2\left[\alpha_1 - t_{11}\left(\varphi_2^e\right)^2 - t_{12}\left(\varphi_1^e\right)^2 - \kappa_{12}\left(\theta_3^e\right)^2\right] - \xi_{44}\frac{\partial^2\delta P_2}{\partial x_1^2} \\ &\quad = t_{44}\delta P_1\varphi_1^e\varphi_2^e, \end{aligned} \tag{6}$$

where stress relation Eq. (4) is used since all the stress components are also small quantities (proportional to $\delta\varphi_1$) near the domain wall. Assuming $\xi_{11} = \xi_{44} = g$ for simplicity, a general solution for this coupled linear equation set is

$$\begin{aligned} \delta P_1 &= 2C_1\cosh(A_1x_1) + 2C_2\sinh(A_2x_1) \\ \delta P_2 &= 2C_1\cosh(A_1x_1) - 2C_2\sinh(A_2x_1), \end{aligned} \tag{7}$$

with constants C_1 and C_2, $A_1 = \sqrt{\frac{2[\alpha_1 - t_{11}(\varphi_1^e)^2 - t_{12}(\varphi_2^e)^2 - \kappa_{12}(\theta_3^e)^2] - t_{44}\varphi_1^e\varphi_2^e}{g}}$ and $A_2 = \sqrt{\frac{2[\alpha_1 - t_{11}(\varphi_1^e)^2 - t_{12}(\varphi_2^e)^2 - \kappa_{12}(\theta_3^e)^2] + t_{44}\varphi_1^e\varphi_2^e}{g}}$. To apply this result to the domain structure in Fig. 1, parameters in different domains are labeled with superscript I, II, or III. Since structural parameters satisfy $|\varphi_1^e| = |\varphi_2^e|$, $\varphi_1^{eI} = -\varphi_1^{eII}$ and $\varphi_2^{eI} = \varphi_2^{eII}$, we have $A_1^I = A_2^{II}$ and $A_2^I = A_1^{II}$. At the I side of the I-II domain wall, distance Δ from the bulk, polarization solutions take the form $\delta P_1 = C_1e^{A_1^I\Delta} + C_2e^{A_2^I\Delta}$, $\delta P_2 = C_1e^{A_1^I\Delta} - C_2e^{A_2^I\Delta}$; at the II side, they are $\delta P_1 = C_1e^{A_2^I\Delta} - C_2e^{A_1^I\Delta}$ and $\delta P_2 = C_1e^{A_2^I\Delta} + C_2e^{A_1^I\Delta}$. However, no nonzero coefficients C_1 and C_2 can be found to simultaneously satisfy the antisymmetric profile of δP_1 together with the symmetric profile of δP_2 observed in experiments. Also, without additional coupling terms, free energy (3) can only generate kinklike or breatherlike profiles, as discussed in Ref. [5] (also shown in Fig. 2), but not the AFE-like odd polarization distribution.

We then perform the phase-field simulation including the effect of flexoelectric coupling. All the simulation settings remain unchanged except that the flexoelectric contribution is added to free energy (2). The contribution of flexoelectricity

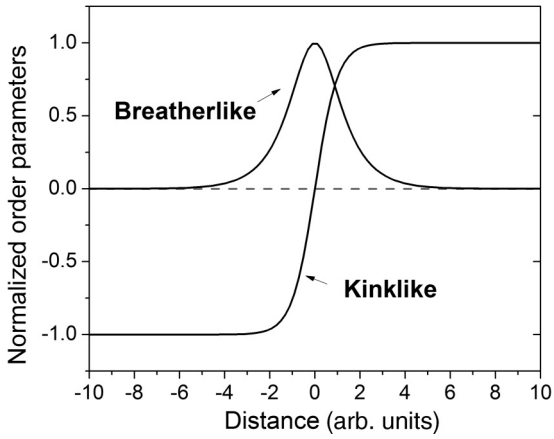

FIG. 2. The schematics of the domain wall profiles for the biquadratic coupling. The profile can be either kinklike or breatherlike.

to the total free energy density can be expressed as

$$f_{\text{flexoelectric}} = \frac{1}{2}f_{ijkl}\left(\frac{\partial P_k}{\partial x_l}\varepsilon_{ij} - \frac{\partial\varepsilon_{ij}}{\partial x_l}P_k\right), \tag{8}$$

where f_{ijkl} is the flexoelectric coupling coefficient. Due to the lack of existing flexoelectric coupling coefficients, we simply pick the typical values [49] for ferroelectric perovskites, i.e., $f_{11} = f_{12} = -10\,\text{C/m}$ and $f_{44} = 0$. The gradient energy coefficients of polarization is renormalized accordingly due to the incorporation of the flexoelectricity [50]. The profiles of order parameters obtained from the simulation are plotted in Fig. 3. The calculated equilibrium values for the structural order parameters are the same as the previous simulation. In addtion, both walls show AFE-like P_1 component at the wall and a ferroelectric P_2 component, which agrees with the previous numerical calculation based on the LGD theory [4]. The wall of polarization is around four pseudocubic unit cells thick, which is wider than the wall of octahedral tilts. Comparing Figs. 3(a) and 3(b), it is found that the P_1 component is invariant with the domain wall structure, while the sign of P_2 is locked with the domain wall angle. This feature can be explained by $P_1 \propto \partial(\varphi_1^2)/\partial x_1$ and $P_2 \propto \partial(\varphi_1\varphi_2)/\partial x_1$ [37]. All the abovementioned characteristics of polar domain walls agree qualitatively well with both previous atomistic calculations [12,14] and experimental observations [11], although the agreement is not quantitative due to the lack of flexoelectric coupling coefficients and the gradient energy coeffiecients. Thus, the flexoelectric coupling can be regarded as, at least, a likely origin of the induced interfacial polar order.

To better undertand the effect of flexoelectric coupling, we carry out an analysis similar to the biquadratic case [Eq. (3) to Eq. (6)]. With the flexoelectric coupling term, an additional term

$$f^B_{\text{flexoelectric}} = \frac{1}{2}F_{12}\left[\frac{\partial P_1}{\partial x_1}(\sigma_{22} + \sigma_{33}) - \frac{\partial(\sigma_{22} + \sigma_{33})}{\partial x_1}P_1\right] \tag{9}$$

is added to Eq. (3). Here, $F_{ij} = s_{ik}f_{kj}$, with i, j, and k running from 1–3. Expressions for the two nonzero stress components in Eq. (4) still holds with $U_2 = R_{12}[(\varphi_1^e)^2 - \varphi_1^2] - Q_{12}P_1^2 - Q_{11}P_2^2 + F_{12}\frac{\partial P_1}{\partial x_1}$ and

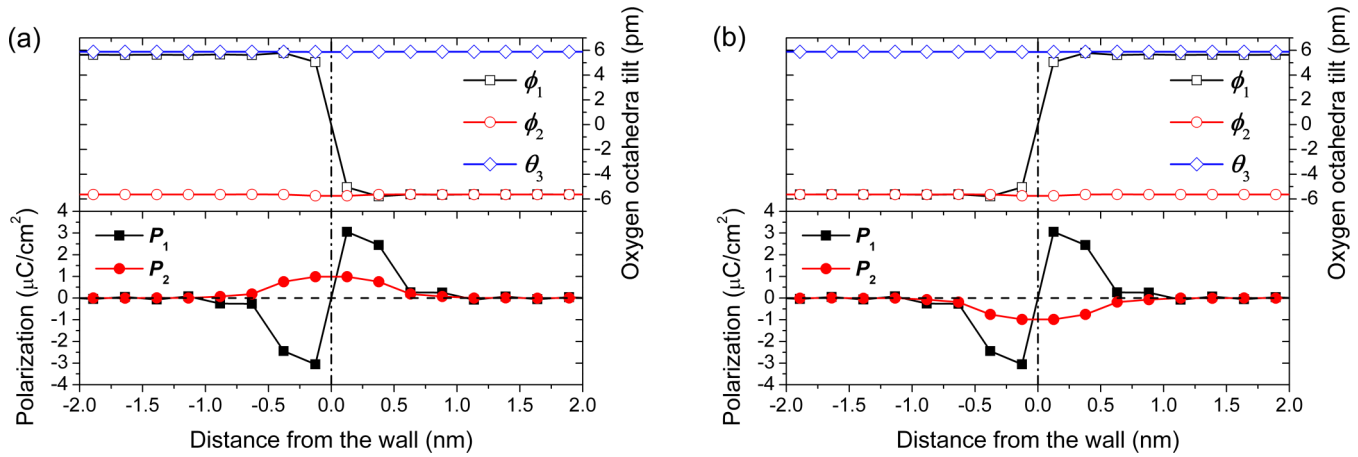

FIG. 3. (Color online) The calculated domain wall profiles from phase-field simulation with flexoelectric contribution. (a) and (b) correspond to the left and right wall, respectively, in Fig. 1. The P_1 component shows an AFE-like profile that is identical in two walls, while the P_2 component changes sign. The profiles of the oxygen octahedra tilt are identical to the phase-field simulation results without including the flexoelectric effect.

$U_3 = R_{12}[(\varphi_1^e)^2 - \varphi_1^2] - Q_{12}(P_1^2 + P_2^2) + F_{12}\frac{\partial P_1}{\partial x_1}$. Minimizing the total energy with respect to P_1 gives an equation similar to Eq. (5a) with an additional term $-F_{12}\frac{\partial(\sigma_{22}+\sigma_{33})}{\partial x_1}$ on the left hand side, while the same result Eq. (5b) is reached for P_2. From here, we take a different approach in analyzing the solution by looking at the linear order expansion of small deviations δP_1 and δP_2 at both sides of the domain wall. For the configuration demonstrated in Fig. 3, the linear order equation is a good approximation at both sides of the wall as long as δP is small (for example at ± 0.75 nm). For δP_1, equations are

$$2A\delta P_1^+ - \xi_{11}\frac{\partial^2 \delta P_1^+}{\partial x_1^2} = F_{12}\frac{\partial(\sigma_{22}^+ + \sigma_{33}^+)}{\partial x_1} \tag{10a}$$

$$2A\delta P_1^- - \xi_{11}\frac{\partial^2 \delta P_1^-}{\partial x_1^2} = F_{12}\frac{\partial(\sigma_{22}^- + \sigma_{33}^-)}{\partial x_1} \tag{10b}$$

with superscript "+" and "−" for different sides of the wall and $A = \alpha_1 - t_{11}(\varphi_1^e)^2 - t_{12}(\varphi_2^e)^2 - \kappa_{12}(\theta_3^e)^2$. To focus on the effect of flexoelectric coupling, we ignore the biquadratic coupling in deriving Eq. (10) (i.e., $t_{44} = 0$). In this case, polarization $\delta P_1^{\pm}$ is determined by the changing rate of stress along x_1. A similar equation for $\delta\varphi_1$ can be written as

$$\begin{aligned} 2\tilde{A}\delta\varphi_1^+ - v_{11}\frac{\partial^2 \delta\varphi_1^+}{\partial x_1^2} + R_{12}(\sigma_{22}^+ + \sigma_{33}^+) = 0 \\ -2\tilde{A}\delta\varphi_1^- + v_{11}\frac{\partial^2 \delta\varphi_1^-}{\partial x_1^2} - R_{12}(\sigma_{22}^- + \sigma_{33}^-) = 0, \end{aligned} \tag{11}$$

where $\delta\varphi_1$ measures the deviation from the bulk value [i.e., $\varphi_1 = -\varphi_1^e + \delta\varphi_1^+$ at the "+" side and $\varphi_1 = \varphi_1^e - \delta\varphi_1^-$ at the "−" side for the setup in Fig. 3(a)] and $\tilde{A} = \beta_1 + \beta_{11}(\varphi_2^e)^2 + 3(\varphi_1^e)^2(\beta_{11} + 2\beta_{12}) - \mu_{12}(\theta_3^e)^2$. Since φ_1 is a known even function, Eq. (11) should give $\delta\varphi_1^+ = \delta\varphi_1^-$, which requires that the stress terms satisfy $\sigma_{22}^+ + \sigma_{33}^+ = \sigma_{22}^- + \sigma_{33}^-$. In Eq. (10), the right-hand sides of Eqs. (10a) and ((10b) have opposite signs because the derivative of an even stress function is an odd function. This indicates that the polarization given by Eq. (10) should satisfy $\delta P_1^+ = -\delta P_1^-$, i.e., an odd polarization profile. These simple observations on the asymptotic polarization behavior near the bulk provide an insight into the effect of flexoelectric coupling and attribute the commonly observed odd polarization profile (or AFE-like) across the domain wall directly to the stress variation and flexoelectric coupling in the system.

As discussed in Ref. [10], the major difference in the flexoelectric coupling and the biquadratic coupling is whether the stress or the stress gradient at the domain wall dominates. As shown above, the width of a domain wall is on the magnitude of nanometers, which give rise to a strain gradient on the magnitude of $10^7\ \mathrm{m}^{-1}$. Such a huge strain gradient makes the flexoelectric effect dominant. For example, it is demonstrated that the additional polarization component to the conventional-believed Ising-like 180° ferroelectric domian walls are driven by the flexoelectric effect [6,39].

Another possible explanation for the origin of polar domain walls is the so-called improper AFD-AFE coupling [12], which is demonstrated universally in perovskites with AFD [51]. The coupled AFE modes include X_5^+ mode (Ca and O atoms at Wyckoff 4c moving along [110]) and R_5^+ mode (Ca atoms moving along $[\bar{1}10]$). To consider the AFD-AFE coupling in $CaTiO_3$, the total free energy needs to include $X_1\varphi_1\theta_3$, $X_2\varphi_2\theta_3$, $R_1\varphi_1\theta_3^2$, and $R_2\varphi_2\theta_3^2$ [51] and some more terms by symmetry [52]. The total free energy with the two AFE modes (X_5^+ and R_5^+) can be written as [12,52,53]

$$\begin{aligned} &f^T(X_1, X_2, R_1, R_2, \varphi_1, \varphi_2, \theta_3) \\ &= \upsilon_1\left(X_1^2 + X_2^2\right) + \upsilon_{11}\left(X_1^2 + X_2^2\right)^2 + \upsilon_{12}\left(X_1^4 + X_2^4\right) + \tau_1\left(R_1^2 + R_2^2\right) + \tau_{11}\left(R_1^2 + R_2^2\right)^2 + \tau_{12}\left(R_1^4 + R_2^4\right) \\ &\quad + \beta_1\left(\varphi_1^2 + \varphi_2^2\right) + \beta_{11}'\left(\varphi_1^2 + \varphi_2^2\right)^2 + \beta_{12}'\left(\varphi_1^4 + \varphi_2^4\right) + \gamma_1\theta_3^2 + (\gamma_{11}' + \gamma_{12}')\theta_3^4 - \mu_{12}'\left(\varphi_1^2 + \varphi_2^2\right)\theta_3^2 \end{aligned}$$

$$+\varpi_X(X_1\varphi_1+X_2\varphi_2)\theta_3+\varpi_R\left(R_1\varphi_1\varphi_2^2+R_2\varphi_2\varphi_1^2\right)+\varpi_\theta\left(R_1\varphi_1\theta_3^2+R_2\varphi_2\theta_3^2\right)+\vartheta_{11}\left(X_1^2+X_2^2\right)\left(R_1^2+R_2^2\right)$$
$$+n_{11}\left(\varphi_1^2+\varphi_2^2\right)\left(X_1^2+X_2^2\right)+\bar{n}_{12}\left(X_1^2+X_2^2\right)\theta_3^2+m_{11}\left(\varphi_1^2+\varphi_2^2\right)\left(R_1^2+R_2^2\right)+\bar{m}_{12}\left(R_1^2+R_2^2\right)\theta_3^2$$
$$+\tfrac{1}{2}\zeta_{11}X_{1,1}^2+\tfrac{1}{2}\zeta_{44}X_{2,1}^2+\tfrac{1}{2}\xi_{11}R_{1,1}^2+\tfrac{1}{2}\xi_{44}R_{2,1}^2+\tfrac{1}{2}v_{11}\varphi_{1,1}^2+\tfrac{1}{2}v_{44}\varphi_{2,1}^2+\tfrac{1}{2}\omega_{44}\theta_{3,1}^2. \quad (12)$$

Since the coefficients of AFD-AFE coupling are not available, we cannot perform numerical simulations. But by using a similar asymptotic analysis as we did for the biquadratic coupling, we find that the signs of X_1 and R_1 are locked with φ_1^e. It simply suggests that the AFE-AFD coupling may capture the polar domain wall features. However, this hypothesis cannot explain the similar AFE-like polarizations at the 180° domain walls of AFD-free tetragonal $BaTiO_3$ [6,39] or $PbTiO_3$ [29,54], which can be well resolved by the flexoelectric effect. The essential difference between the flexoelectric coupling and the improper AFD-AFE coupling is that the former describes the interaction between the optical mode (polarization) and the acoustic mode (AFD), while the latter describes the competition between two acoustic modes (AFE and AFD). As demonstrated by first-principles calculations [55], the optical mode is inherently unstable in $CaTiO_3$. Simply by manipulating the epitaxial strain, the AFD can be suppressed and thus gives rise to polarization [42,55]. Therefore, it is reasonable to conclude that the emergence of AFE-like polarization at the domain wall is due to the inherent instability of the optical mode; however, more experimental and theoretical studies are needed to further clarify the mechanism.

To summarize, employing the phase-field modeling and asymptotic analysis we investigated the origin of the polar domain walls in incipient ferroelectric $CaTiO_3$ by including several coupling terms in the Landau-Ginzburg-Davonshire theory. It is shown that the biquadratic coupling of AFD and polarization alone is unable to produce all the key features of the polarization at the domain walls, while the domain wall structures generated by the flexoelectric coupling agree qualitatively with both previous calculations and experimental observations. The improper AFD-AFE coupling may also give rise to the complex polarization distribution at the domain wall, but it ignores the instability of the optical mode (polarization) and cannot explain the similar polarization profiles of the pure ferroelectric domain walls. However, further studies are still needed to exclude this possibility.

This paper was supported by the National Science Foundation (NSF) through Grants No. DMR-1410714, No. DMR-1210588, and No. DMR 1234096. The computer simulations were carried out on the LION and Cyberstar clusters at the Pennsylvania State University, in part supported by instrumentation (Cyberstar Linux cluster) funded by the NSF through Grant No. OCI-0821527.

[1] D. Meier, J. Seidel, A. Cano, K. Delaney, Y. Kumagai, M. Mostovoy, N. A. Spaldin, R. Ramesh, and M. Fiebig, Nat. Mater. **11**, 284 (2012).
[2] J. Seidel, L. W. Martin, Q. He, Q. Zhan, A. Rother, M. E. Hawkridge, P. Maksymovych, P. Yu, M. Gajek, N. Balke, S. V. Kalinin, S. Gemming, F. Wang, G. Catalan, J. F. Scott, N. A. Spaldin, J. Orenstein, R. Ramesh, and Y. H. Chu, Nat. Mater. **8**, 229 (2009).
[3] E. A. Eliseev, A. N. Morozovska, G. S. Svechnikov, P. Maksymovych, and S. V. Kalinin, Phys. Rev. B **85**, 045312 (2012).
[4] E. A. Eliseev, A. N. Morozovska, Y. Gu, A. Y. Borisevich, L.-Q. Chen, V. Gopalan, and S. V. Kalinin, Phys. Rev. B **86**, 085416 (2012).
[5] B. Houchmandzadeh, J. Lajzerowicz, and E. K. H. Salje, J. Phys.: Condens. Matter **3**, 5163 (1991).
[6] P. V. Yudin, A. K. Tagantsev, E. A. Eliseev, A. N. Morozovska, and N. Setter, Phys. Rev. B **86**, 134102 (2012).
[7] M. Calleja, M. T. Dove, and E. K. H. Salje, J. Phys.: Condens. Matter **15**, 2301 (2003).
[8] L. Goncalves-Ferreira, S. A. T. Redfern, E. Artacho, E. Salje, and W. T. Lee, Phys. Rev. B **81**, 024109 (2010).
[9] J. F. Scott, E. K. H. Salje, and M. A. Carpenter, Phys. Rev. Lett. **109**, 187601 (2012).
[10] E. K. H. Salje, O. Aktas, M. A. Carpenter, V. V. Laguta, and J. F. Scott, Phys. Rev. Lett. **111**, 247603 (2013).
[11] S. Van Aert, S. Turner, R. Delville, D. Schryvers, G. Van Tendeloo, and E. K. H. Salje, Adv. Mater. **24**, 523 (2012).
[12] P. Barone, D. Di Sante, and S. Picozzi, Phys. Rev. B **89**, 144104 (2014).
[13] H. Yokota, H. Usami, R. Haumont, P. Hicher, J. Kaneshiro, E. K. H. Salje, and Y. Uesu, Phys. Rev. B **89**, 144109 (2014).
[14] L. Goncalves-Ferreira, S. A. T. Redfern, E. Artacho, and E. K. H. Salje, Phys. Rev. Lett. **101**, 097602 (2008).
[15] G. Catalan, J. Seidel, R. Ramesh, and J. F. Scott, Rev. Mod. Phys. **84**, 119 (2012).
[16] A. Aird and E. K. H. Salje, J. Phys.: Condens. Matter **10**, L377 (1998).
[17] J. Guyonnet, I. Gaponenko, S. Gariglio, and P. Paruch, Adv. Mater. **23**, 5377 (2011).
[18] W. J. Merz, Phys. Rev. **95**, 690 (1954).
[19] S. S. P. Parkin, M. Hayashi, and L. Thomas, Science **320**, 190 (2008).
[20] T. Sluka, A. K. Tagantsev, P. Bednyakov, and N. Setter, Nat. Commun. **4**, 1808 (2013).
[21] R. Xu, J. Karthik, A. R. Damodaran, and L. W. Martin, Nat. Commun. **5**, 3120 (2014).
[22] X.-K. Wei, A. K. Tagantsev, A. Kvasov, K. Roleder, C.-L. Jia, and N. Setter, Nat. Commun. **5**, 3031 (2014).
[23] R. K. Vasudevan, W. Wu, J. R. Guest, A. P. Baddorf, A. N. Morozovska, E. A. Eliseev, N. Balke, V. Nagarajan, P. Maksymovych, and S. V. Kalinin, Adv. Funct. Mater. **23**, 2592 (2013).
[24] Q. Zhang and W. A. Goddard, Appl. Phys. Lett. **89**, 182903 (2006).

[25] Y.-H. Shin, I. Grinberg, I.-W. Chen, and A. M. Rappe, Nature **449**, 881 (2007).
[26] M. Taherinejad, D. Vanderbilt, P. Marton, V. Stepkova, and J. Hlinka, Phys. Rev. B **86**, 155138 (2012).
[27] J. C. Wojdeł and J. Íñiguez, Phys. Rev. Lett. **112**, 247603 (2014).
[28] E. A. Eliseev, P. V Yudin, S. V. Kalinin, N. Setter, A. K. Tagantsev, and A. N. Morozovska, Phys. Rev. B **87**, 054111 (2013).
[29] D. Lee, R. K. Behera, P. Wu, H. Xu, Y. L. Li, S. B. Sinnott, S. R. Phillpot, L. Q. Chen, and V. Gopalan, Phys. Rev. B **80**, 060102(R) (2009).
[30] B. Meyer and D. Vanderbilt, Phys. Rev. B **65**, 104111 (2002).
[31] A. N. Morozovska, R. K. Vasudevan, P. Maksymovych, S. V Kalinin, and E. A. Eliseev, Phys. Rev. B **86**, 085315 (2012).
[32] J. Padilla, W. Zhong, and D. Vanderbilt, Phys. Rev. B **53**, R5969 (1996).
[33] D. A. Scrymgeour, V. Gopalan, A. Itagi, A. Saxena, and P. J. Swart, Phys. Rev. B **71**, 184110 (2005).
[34] Y. Wang, C. Nelson, A. Melville, B. Winchester, S. Shang, Z.-K. Liu, D. G. Schlom, X. Pan, and L.-Q. Chen, Phys. Rev. Lett. **110**, 267601 (2013).
[35] M. E. Lines and A. M. Glass, *Principles and Applications of Ferroelectrics and Related Materials* (Oxford University Press, Oxford, 1977).
[36] F. Jona and G. Shirane, *Ferroelectric Crystals* (Dover Publications Inc., Mineola, New York, 1993).
[37] A. N. Morozovska, E. A. Eliseev, M. D. Glinchuk, L.-Q. Chen, and V. Gopalan, Phys. Rev. B **85**, 094107 (2012).
[38] A. N. Morozovska, E. A. Eliseev, S. V. Kalinin, L.-Q. Chen, and V. Gopalan, Appl. Phys. Lett. **100**, 142902 (2012).
[39] Y. Gu, M. Li, A. N. Morozovska, Y. Wang, E. A. Eliseev, V. Gopalan, and L.-Q. Chen, Phys. Rev. B **89**, 174111 (2014).
[40] A. P. Levanyuk and D. G. Sannikov, Sov. Phys. Uspekhi **17**, 199 (1974).
[41] R. Ahluwalia, A. K. Tagantsev, P. Yudin, N. Setter, N. Ng, and D. J. Srolovitz, Phys. Rev. B **89**, 174105 (2014).
[42] Y. Gu, K. Rabe, E. Bousquet, V. Gopalan, and L.-Q. Chen, Phys. Rev. B **85**, 064117 (2012).
[43] L.-Q. Chen, Annu. Rev. Mater. Res. **32**, 113 (2002).
[44] A. G. Khachaturyan, *Theory of Structural Transformations in Solids* (Dover Publications Inc., Mineola, New York, 2008), p. 576.
[45] Y. L. Li, S. Y. Hu, Z. K. Liu, and L. Q. Chen, Appl. Phys. Lett. **81**, 427 (2002).
[46] M. Yashima and R. Ali, Solid State Ionics **180**, 120 (2009).
[47] B. J. Kennedy, C. J. Howard, and B. C. Chakoumakos, J. Phys.: Condens. Matter **11**, 1479 (1999).
[48] N. Wang, R. Spatschek, and A. Karma, Phys. Rev. E **81**, 051601 (2010).
[49] J. Hong and D. Vanderbilt, Phys. Rev. B **88**, 174107 (2013).
[50] A. K. Tagantsev, E. Courtens, and L. Arzel, Phys. Rev. B **64**, 224107 (2001).
[51] L. Bellaiche and J. Íñiguez, Phys. Rev. B **88**, 014104 (2013).
[52] H. T. Stokes and D. M. Hatch, Stokes.byu.edu/isotropy.html (n.d.).
[53] C.-J. Eklund, *Interplay of Strain, Polarization, and Magnetic Ordering in Complex Oxides from First Principles* (Rutgers University, Piscataway, NJ, 2010).
[54] R. K. Behera, C. Lee, D. Lee, A. N. Morozovska, S. B. Sinnott, A. Asthagiri, V. Gopalan, and S. R. Phillpot, J. Phys.: Condens. Matter **23**, 175902 (2011).
[55] C.-J. Eklund, C. J. Fennie, and K. M. Rabe, Phys. Rev. B **79**, 220101(R) (2009).